New Insights into the Mechanism of Nucleoside Hydrolases from the Crystal Structure of the Escherichia coli YbeK Protein Bound to the Reaction Product † , ‡

ARTICLE *in* BIOCHEMISTRY · FEBRUARY 2006

Impact Factor: 3.02 · DOI: 10.1021/bi0511991 · Source: PubMed

New Insights into the Mechanism of Nucleoside Hydrolases from the Crystal Structure of the *Escherichia coli* YbeK Protein Bound to the Reaction Product[†,‡]

Laura Muzzolini,[§,||] Wim Versées,[⊥] Paola Tornaghi,[§] Els Van Holsbeke,[⊥] Jan Steyaert,[⊥] and Massimo Degano*[,§]

Biocrystallography Unit, DIBIT Scientific Institute S. Raffaele, via Olgettina 58, 20132 Milan, Italy, and Department of Cellular and Molecular Interactions, Vlaams Interuniversitair Instituut voor Biotechnologie, Vrije Universiteit Brussel, Pleinlaan 2, 1050 Brussels, Belgium

Received June 22, 2005; Revised Manuscript Received November 12, 2005

ABSTRACT: Nucleoside hydrolases (NHs) are enzymes that catalyze the excision of the N-glycosidic bond in nucleosides to allow recycling of the nitrogenous bases. The fine details of the catalytic mechanism and the structural features imposing the substrate specificity of the various members of the NH family are still debated. Here we present the functional characterization of the *Escherichia coli* YbeK (RihA) protein as a pyrimidine nucleoside-preferring NH and its first crystal structure to 1.8 Å resolution. The enzyme active site is occupied by either the α or *β* anomer of ribose and provides the first structural description of the binding of the NH reaction product. While the amino acid residues involved in ribosyl binding are strictly conserved in pyrimidine-specific NHs, the residues involved in specific interactions with the nitrogenous bases differ considerably. Further comparison of the active site architecture of YbeK with the related NHs establishes structural determinants involved in triggering the conformational transition between the open and closed structures and suggests a mechanism for product release.

In all organisms nucleic acids undergo an active turnover mediated by diverse catabolic reactions that ultimately lead to the liberation of the nitrogenous bases. The free purines and pyrimidines can then react with PRPP to form the correspondent nucleotides, with an overall lower energy requirement compared to de novo synthesis (*1*). Although these salvage pathways are diverse in character and distribution among organisms, the step involving the release of the bases from free nucleosides is apparently conserved and is catalyzed by either nucleoside phosphorylases (NPs)[1] (*2*) or nucleoside hydrolases (NHs) (*3*). Members of the NP family are key enzymes in nucleotide salvage both in prokaryotes and in eukaryotes, catalyzing the reversible phosphorolysis of the C−N glycosidic bond of purine and pyrimidine nucleosides to yield the free base and ribose 1-phosphate. In contrast, NHs are glycosidases that catalyze the substantially irreversible hydrolysis of the N-glycosidic bond of *β*-ribonucleosides, releasing the nitrogenous base and ribose through the reaction:

$$\text{Pur/Pyr nucleoside} + H_2O \leftrightarrow \text{Pur/Pyr base} + \text{ribose}$$

NHs (EC 3.2.2.-) are a family of structurally and functionally related metalloproteins (*4*) initially identified and characterized in parasitic protozoa such as *Trypanosoma* (*5*) and *Crithidia* (*6*). NHs have a well-established, fundamental metabolic role in the nucleoside salvage pathways of these purine-auxotrophic organisms, since they often also lack the NPs found in prokaryotes and higher eukaryotes (*3*). NHs are, however, not confined to protozoa, since nucleoside hydrolase activity has also been characterized in other organisms such as bacteria (*7*, *8*), yeast (*9*), insects (*10*), and nematodes (*11*), whereas it has never been observed in mammals. The physiological role of these nonprotozoan NHs is not immediately apparent, given the known role of NPs in nucleobase salvage (*12*). These reports suggest a specialized function for some NH enzymes, such as adenosine degradation as a means of reducing the perception of micropredation by the host in the mosquito *Aedes aegypti* (*10*), or prevention of sporulation by inosine in the spore-forming bacteria *Bacillus cereus* (*13*) and *Bacillus anthracis* (*14*). Conversely, the colocalization of the *Escherichia coli* NH-like gene *yeiK/rihB* with nucleoside transporters or other nucleotide-metabolizing enzymes suggests a role in nucleotide metabolism (*15*).

Four classes of NHs have been identified on the basis of their substrate specificity: the nonspecific IU-NHs which

[†] Supported by research grants from the Italian Association for Cancer Research (M.D.), FIRB-Italian Basic Research Funding (M.D.), Cariplo Foundation (M.D.), and the IWT-Vlaanderen (J.S.). W.V. thanks the Fund for Scientific Research-Flanders (FWO-Vlaanderen) for a postdoctoral grant.

[‡] The coordinates and structure factors of the YbeK/ribose complex have been deposited with the Protein Data Bank, accession code 1YOE.

* Corresponding author. Tel: +39-022643-7152. Fax: +39-022643-4153. E-mail: degano.massimo@hsr.it.

[§] DIBIT Scientific Institute S. Raffaele.

[||] Present address: Proteomics, International Centre for Genetic Engineering and Biotechnology, Padriciano 99, Trieste, Italy.

[⊥] Vrije Universiteit Brussel.

[1] Abbreviations: NP, nucleoside phosphorylase; NH, nucleoside hydrolase; IU-NH, inosine−uridine-preferring nucleoside hydrolase; CU-NH, cytidine−uridine-preferring nucleoside hydrolase; IAG-NH, inosine−adenosine−guanosine-preferring nucleoside hydrolase; TB, terrific broth; IPTG, isopropyl *β*-thiogalactopyranoside; Tris, tris-(hydroxyethyl)aminomethane; AEBSF, 4-(2-aminoethyl)benzenesulfonyl fluoride; NTA, nitriloacetic acid; Hepes, 4-(2-hydroxyethyl)-1-piperazineethanesulfonic acid; pNPR, 4-nitrophenyl ribopyranoside; DLS, dynamic light scattering; MPD, 2-methyl-2,4-pentanediol; SDS−PAGE, sodium dodecyl sulfate−polyacrylamide gel electrophoresis; pAPIR, 1-(4-aminophenyl)-2-hydroxypyrrolidine-3,4-diol; rmsd, root mean square distance.

10.1021/bi0511991 CCC: $33.50
Published on Web 12/23/2005

hydrolyze both purine and pyrimidine nucleosides (*16*), the purine-specific IAG-NHs (*17*, *18*), the 6-oxopurine-specific GI-NHs (*19*), and finally the pyrimidine nucleoside-specific CU-NHs (*20*). On the basis of their sequence identity and the conservation of key amino acid residues, the NH sequences in the various databases seem to fall into three distinct groups with IU- and CU-NHs belonging to group I, IAG-NHs to group II, and a yet uncharacterized subfamily to group III (*21*). The first structural information on NHs was obtained from the crystal structures of the group I IU-NH from *Crithidia fasciculata*, both unliganded (*22*) and in complex with a transition state-like inhibitor (*23*). These structures have highlighted two main features of the NH family, namely, an open (α/β) fold and the presence of a divalent calcium ion bound at the active site that is involved in both substrate binding and catalysis. A cluster of aspartic acid residues at the N-terminus of the enzyme (DXDXXXDD) actively participates in both ion coordination and crucial interactions with the substrate and is thus considered a fingerprint for proteins with NH activity. The three-dimensional structure of the IAG-NH (*24*) from *Trypanosoma vivax* demonstrated that the same structural framework evolved to an active site highly optimized for binding and hydrolysis of purine nucleosides. The structure of a CU-NH enzyme showed instead a strong similarity with the nonspecific isozymes, but the structural basis for the strict pyrimidine nucleoside specificity is yet unresolved.

Three NH-like genes have been identified in the genome of *E. coli*, two encoding for CU-NHs, *ybeK* (*rihA*) and *yeiK* (*rihB*), and one for an IU-NH, *yaaF (*r*ihC*) (*7*). The exact physiological role of these enzymes in wild-type *E. coli* is still enigmatic, since their activities are paralleled by the NPs. However, the *ybeK* gene product constitutes the major pathway of cytidine utilization in the pyrimidine-requiring cytidine deaminase (*cdd*) mutants of *E. coli*. The enzyme was also found to be a contributor to the pathway of uridine salvage operating in the absence of uridine kinase and uridine phosphorylase. The crystal structure of YeiK provided the first structural description of a pyrimidine-specific NH (*21*). YeiK displays the group I NH fold, and the active site of the enzyme is more similar in structure and composition to the IU-NH rather than to the IAG-NH enzymes. However, it is still unknown which active site amino acids are responsible for the preference toward pyrimidine nucleosides of the CU-NHs as compared to the IU-NHs. Moreover, the details of the enzymatic mechanism of the reaction catalyzed by CU-NHs are still elusive.

Here we present the enzymatic characterization and high-resolution X-ray crystallographic analysis of *E. coli* YbeK nucleoside hydrolase bound to the reaction product D-ribose. The YbeK gene product is an NH enzyme with marked specificity toward pyrimidine nucleosides. The 1.8 Å crystal structure represents the first structural characterization of an NH enzyme in complex with the product of the hydrolytic reaction.

MATERIALS AND METHODS

Cloning, Expression, and Purification. The *ybeK* gene (936 bp) was amplified by polymerase chain reaction from genomic DNA of the *E. coli* K12 strain. The gene was amplified using the forward primer 5′-CGAGATCTGCACTGCCAATTCTGT-3′ and the reverse primer 5′-TATAAGCTTAAGCGTAAAATTTCAGACGATCAGGC-3′, resulting in the deletion of the ATG initiation codon and in the introduction of *Bgl*II and *Hin*dIII sites at the 5′ and 3′ ends of the gene, respectively. This amplified fragment was cloned in the *Bam*HI and *Hin*dIII sites of the multicloning site of the pQE-30 (Qiagen) expression plasmid vector, in frame with an N-terminal hexahistidine tag. The coding sequence was verified by dideoxy chain-termination sequencing of both DNA strands. The resulting recombinant plasmid was transformed into *E. coli* WK6 for overexpression.

Cells were grown in TB medium containing 50 μg/mL ampicillin at 37 °C to an OD_{600} of 0.6. The medium was then cooled to 28 °C, and isopropyl β-thiogalactopyranoside (IPTG) was added to a final concentration of 0.5 mM to induce expression of recombinant YbeK. Bacteria were harvested after 16 h by centrifugation and resuspended in 20 mM Tris, pH 7.5, 10 mM imidazole, and 1 M NaCl with the added protease inhibitors leupeptin (1 $\mu g \cdot mL^{-1}$) and 4-(2-aminoethyl)benzenesulfonyl fluoride (AEBSF, 0.1 $mg \cdot mL^{-1}$). The cells were lysed via three consecutive passages through a French pressure cell. The soluble fraction after centrifugation was loaded on a 5 mL Ni-NTA column (Qiagen). After extensive washing with 20 mM Tris, pH 7.5, 10 mM imidazole, and 1 M NaCl, proteins were eluted using a buffer containing 20 mM Tris, pH 7.5, 0.5 M imidazole, and 1 M NaCl. The relevant fractions were pooled and run over a preparative Superdex-200 gel filtration column (Amersham Biosciences) in 20 mM Tris, pH 7.0, 150 mM NaCl, and 1 mM $CaCl_2$. The purified protein was homogeneous as judged from Coomassie-stained SDS−PAGE.

Quaternary Structure Determination. Analytical size exclusion chromatography was performed on a Superdex-200 column coupled to an AKTA Purifier-10 instrument (Amersham Biosciences). Proteins were eluted isocratically using a buffer containing 20 mM Hepes, pH 7.4, and 300 mM NaCl. The retention factor K_d was calculated from the formula $K_d = (V_e - V_0)/(V_c - V_0)$, where V_e, V_0, and V_c are the elution, void, and column volumes, respectively. A calibration curve was obtained from the retention factors of known molecular weight standards. Dynamic light scattering measurements were carried out on a DynaPro MS/X instrument (Protein Solutions, Inc.), scanning different temperatures in the range between 4 and 37 °C and protein concentrations between 0.01 and 10 $mg \cdot mL^{-1}$ in a buffer containing 20 mM Hepes and 150 mM KCl, pH 7.4. The DYNAMICS v6 software was used to calculate an autocorrelation function to fit the measurements to either a monomodal or bimodal distribution. The resultant autocorrelation function data were analyzed to obtain an average particle diameter, and molecular mass values were calculated using a standard molecular weight curve.

Enzymatic Assays. The specific activity and kinetic parameters of YbeK for the nucleosides adenosine, guanosine, inosine, cytidine, and uridine were determined with the modified reducing sugar colorimetric assay as previously described (*16*). Hydrolysis of *p*-nitrophenyl riboside (pNPR) was monitored spectrophotometrically at 400 nm using an extinction coefficient of 12 $mM^{-1} \cdot cm^{-1}$ under the assay conditions. All measurements were carried out at 35 °C in 50 mM phosphate buffer, pH 7.0. All kinetic parameters were

Table 1: Steady-State Kinetic Parameters for YbeK (Present Work) and YeiK (*21*)[a]

	YbeK			YeiK		
substrate	k_{cat} (s^{-1})	K_M (μM)	k_{cat}/K_M (M^{-1} s^{-1})	k_{cat} (s^{-1})	K_M (μM)	k_{cat}/K_M (M^{-1} s^{-1})
guanosine	0.0056 ± 0.0002	363 ± 61	$(1.5 \pm 0.3) \times 10^1$			
adenosine	0.0154 ± 0.0005	648 ± 69	$(2.4 \pm 0.3) \times 10^1$			
inosine	0.043 ± 0.005	239 ± 131	$(1.8 \pm 1.1) \times 10^2$			
cytidine	11.6 ± 0.6	524 ± 82	$(2.2 \pm 0.4) \times 10^4$	11.6 ± 1.8	532 ± 101	$(2.2 \pm 0.7) \times 10^4$
uridine	13.9 ± 0.4	83 ± 12	$(1.7 \pm 0.2) \times 10^5$	4.7 ± 0.1	142 ± 8	$(3.3 \pm 0.2) \times 10^4$
pNPR	39 ± 2	180 ± 18	$(2.2 \pm 0.2) \times 10^5$			

[a] Kinetic constants were determined from direct fits of the experimental data to the Michaelis−Menten equation.

calculated per active site, making them independent of the multimerization state of the enzyme.

Crystallization and Data Collection. Crystals of the YbeK/ribose complex were obtained by hanging drop vapor diffusion at 20 °C. A 10 mg·mL^{-1} YbeK solution in 10 mM Tris, pH 7.0, 25 mM NaCl, and 500 mM ribose was mixed with equal volumes of a precipitant solution containing 24% MPD, 0.1 M sodium acetate, pH 5.0, and 500 mM ribose. Crystals were visible within 1 week and grew to maximum dimensions of 500 × 200 × 100 μm. For data collection, crystals were mounted in nylon-fiber loops and flash-cooled in a dry nitrogen stream at 100 K. A buffer containing 30% MPD, 0.1 M sodium acetate, pH 5.0, and 500 mM ribose was used as cryoprotectant. Diffraction data were collected at beamline ID14-EH2 of the European Synchrotron Radiation Facility (Grenoble, France) on a Quantum4 CCD detector using the oscillation method and an X-ray wavelength of 0.933 Å. Data were indexed, integrated, and scaled using programs from the HKL package (*25*), and measured intensities were converted to structure factor amplitudes using the program TRUNCATE (*26*), part of the CCP4 suite (*27*). The crystals belong to the orthorhombic *I*222 (or $I2_12_12_1$) space group, with unit cell dimensions $a = 76.5$ Å, $b = 84.1$ Å, and $c = 112.5$ Å. The cell volume is consistent with one YbeK monomer present in the asymmetric unit, with 52% solvent and a Matthews' coefficient of 2.6 Å^3/Da (*28*).

Structure Solution and Refinement. The structure of YbeK was solved by the molecular replacement technique as implemented in the program MOLREP (*29*) using one monomer of the CU-NH YeiK from *E. coli* (PDB code 1Q8F) as the search model after removal of all solvent molecules, ligands, and ions. The model shares 39% amino acid sequence identity with YbeK. Rotation and translation functions yielded a single solution in space group *I*222. The crystallographic *R*-factor after 20 cycles of rigid body refinement of the model was 0.51, calculated on all data up to 3.0 Å. An initial electron density map calculated with $2F_o - F_c$ coefficients and model phases up to 1.8 Å resolution was visually inspected to confirm the correctness of the solution. The structure of YbeK was traced using the ARP/wARP package (*30*). Manual rebuilding in sigmaA-weighted ($2F_o - F_c$, ϕ_c) and ($F_o - F_c$, ϕ_c) electron density maps using the program O (*31*) and restrained maximum-likelihood positional and isotropic temperature factor refinement with REFMAC5 (*32*) were performed in a cyclic process of gradual improvement of the model. SigmaA-weighted "shake" ($2F_o - F_c$, ϕ_c) and ($F_o - F_c$, ϕ_c) omit maps were inspected to allow modeling of difficult regions to minimize phase bias (*33*). Modeling of anisotropic motion for the entire molecule as a single group of atoms was achieved by refining the translation, libration, and screw axis (TLS) displacement tensors (*34*). After the *R*-factor decreased below 0.23, water molecules were added to the model using the ARP/wARP package (*30*). The accuracy of solvent building was assessed by visual inspection and applying a cutoff on *B*-factors of 50 Å^2. The crystallographic R_{crys} and R_{free} values converged to 0.164 and 0.186. During refinement, the geometry of the model was monitored with PROCHECK (*35*) and WHAT_CHECK (*36*). Root mean square deviations (rmsd) and molecular superpositions were computed with the program LSQMAN (*37*). Buried surface areas were calculated with the program SC (*38*).

After the first macrocycle of refinement a ribose molecule was fitted in the YbeK active site according to the ($F_o - F_c$, ϕ_c) electron density map calculated at 1.8 Å resolution. We initially interpreted the density with the most populated β-furanose form of D-ribose. However, positive residual electron density below the ribose ring at the C1′ atom persisted after several rounds of refinement and could only be justified by the concomitant presence of the α anomer of the sugar in the crystal. The disappearance of this residual density in ($F_o - F_c$, ϕ_c) maps after refinement supported this interpretation of the data. The atom occupancy of each anomer was initially set to 50% and afterward varied systematically, keeping the sum equal to 1.0, and refined against the diffraction data. The final ratio of 35% β- and 65% α-D-ribose bound to the YbeK crystal active sites was achieved from optimal fitting of the ($2F_o - F_c$, ϕ_c) maps, minimization of the ($F_o - F_c$, ϕ_c) residual electron density, and correlation of the atomic temperature factors with the surrounding protein atoms after refinement (Supporting Information, Figure 1).

RESULTS AND DISCUSSION

Pyrimidine-specific NHs (CU-NHs) are a long-known class of enzymes that are found in both prokaryotes and eukaryotes, yet only in recent years are receiving increased attention. Indeed, their physiological role is yet debated, since they appear to perform a redundant role in nucleotide metabolism that is paralleled by the activity of well-characterized enzymes, such as NPs. The marked sequence homology between nonspecific and pyrimidine-specific NHs, including the active site residues that can confer substrate specificity, suggests a divergent evolution from a common ancestor. In this work we characterized the recombinant *E. coli* YbeK enzyme, a member of the group I NHs, as a pyrimidine-specific NH.

Kinetic Properties of YbeK, a Second Pyrimidine-Specific NH from E. coli. The steady-state kinetic parameters of the purified hexahistidine-tagged YbeK (Table 1) show that this enzyme hydrolyzes the naturally occurring pyrimidine nu-

cleosides 100−10000 times more efficiently than the purine nucleosides. Among the pyrimidines, uridine is converted most efficiently with a 10 times higher k_{cat}/K_M than cytidine mainly owing to a lower K_M value. This higher affinity for uridine might indicate the presence of a ground-state interaction between the enzyme and the 4-keto or N3 of the uracil ring. The low specificity of YbeK for the purines is caused by a lower turnover of these compounds, while the K_M values are in the same order of magnitude as for the pyrimidines. This finding implies that the discrimination against purines is not due to a mere steric exclusion of the bulkier purine ring but rather to a specific interaction in the transition state between the enzyme and the pyrimidine ring, not possible with the purines. Since this "catalytic" interaction takes place with both cytidine and uridine, the 2-keto group is most likely involved in the catalytic mechanism. Comparison between YbeK and YeiK shows that the steady-state kinetic parameters for the natural substrate cytidine are remarkably similar in both enzymes (Table 1). The differences in catalytic activities of the two CU-NHs on the substrate uridine, affecting both K_M and k_{cat} values, reflect a difference of only 1.0 kcal·mol^{-1} in lowering the transition state barrier. Hence, the YbeK and YeiK enzymes achieve comparable levels of transition state stabilization, despite the fact that protein/nitrogenous base interactions are mediated by different amino acids.

Comparing the kinetic parameters of the natural pyrimidine nucleosides of YbeK with those for the substrate analogue pNPR is indicative for the effectiveness of leaving group activation by the enzyme. The low pK_a of the *p*-nitrophenolate leaving group (around 7) makes leaving group activation unnecessary in the latter substrate, and therefore the enzymatic hydrolysis of this compound only relies on activation of the nucleophile (water) and stabilization of the oxocarbenium ion in the transition state (*39*, *40*). The k_{cat} values for both pyrimidine nucleosides are only a factor of 3 lower compared to pNPR, meaning that the enzyme efficiently activates the pyrimidine bases in catalysis. The rate enhancement of pNPR hydrolysis by YbeK, comparing the reaction rates of the catalyzed and uncatalyzed reactions (*39*), amounts to a $\Delta\Delta G^{\ddagger}$ of −12.9 kcal·mol^{-1}. From the existing data on 2′-deoxynucleosides (*41*) and taking into account that the hydrolysis of nucleosides is at least 100-fold slower (*42*), the rate of solvolysis of pyrimidine nucleosides can be approximated to 10^{-12} s^{-1}. This value allows the computation of an approximate $\Delta\Delta G^{\ddagger}$ of −18.7 kcal·mol^{-1} as the total contribution of enzymatic forces for the reaction rate enhancement by YbeK, comparable to what was observed for the *Crithidia* IU-NH (*43*). Thus, the remaining energy difference of −5.8 kcal·mol^{-1} can be ascribed to the activation of the leaving group by the enzyme that could be readily achieved through proton transfer but also via specific hydrogen bonding.

YbeK Displays the Group I NH Fold and Tetrameric Structure. The crystal structure of YbeK was solved by molecular replacement using the YeiK nucleoside hydrolase from *E. coli* as a search model. The structure was refined against diffraction data to 1.8 Å resolution to R_{crys} and R_{free} values of 0.164 and 0.186, respectively (Table 2). A single YbeK polypeptide chain is present in the asymmetric unit. The final model contains 302 amino acid residues of a total of 312 in 1 YbeK monomer, 215 water molecules, 1 Ca^{2+} ion, and 1 ribose molecule. Two amino acid stretches, between Asp79 and Gly83 and between Tyr226 and Glu230, could not be located in electron density maps and were thus omitted from the final model. Eight amino acids with alternate side chain conformations were identified, and both conformers are included in the final model.

Table 2: Crystallographic Data Collection and Refinement Statistics

data collection statistics	
wavelength (Å)	0.933
resolution range (Å)[a]	24.4−1.78 (1.86−1.78)
no. measured reflections	426060
no. unique reflections	34056
completeness (%)[a]	97.6 (77.4)
redundancy	12.5
R_{sym}[a,b]	0.116 (0.455)
$I/\sigma(I)$[a]	26.2 (2.9)
refinement statistics	
resolution range (Å)[a]	24.4−1.78 (1.86−1.78)
cutoff used	$F_o > 0$
no. of reflections[a]	32970 (1847)
reflections for cross-validation[a]	1086 (63)
total no. of atoms	2565
R_{crys}[a,c]	0.164 (0.189)
R_{free}[a,c]	0.186 (0.252)
rmsd bond lengths (Å)	0.009
rmsd bond angles (deg)	1.303
coordinate error (Å) based on R_{crys}	0.102
Ramachandran plot (% residues)	
most favored regions	90.1
additionally allowed regions	9.9
generously allowed or disallowed regions	0.0
average temperature factors (Å^2)	
protein atoms	14.0
water molecules	30.9
ligand atoms	14.4

[a] Values in parentheses refer to the highest resolution shell. [b] $R_{sym} = \sum_{hkl}\sum_i|I_i(hkl) - \langle I(hkl)\rangle|/\sum_{hkl}I_i(hkl)$, where $I_i(hkl)$ and $\langle I(hkl)\rangle$ are the intensity of the *ith* measurement and the average intensity value for reflection *hkl*, respectively. [c] $R = \sum_{hkl}||F_o(hkl)| - |F_c(hkl)||/\sum_{hkl}|F_o(hkl)|$, where F_o and F_c are the observed and calculated structure factors for the reflection *hkl* and the summation is extended over all reflections used in the refinement. For R_{free}, the value is calculated using a randomly selected subset of reflections excluded from the minimization throughout refinement.

The YbeK monomer is folded into a single domain structure containing 11 α-helices and 10 β-strands. The overall structure resembles the NH fold (*22*), with an open (α/β) structure. The core of the enzyme contains a characteristic eight-stranded central β-sheet, with seven parallel strands and one antiparallel strand, and six intervening α-helices. The active site of YbeK is located in a deep cavity at the C-terminal end of the central β-sheet and is capped by four α-helices (Figure 1). In the present structure a ribose molecule is bound to the catalytic Ca^{2+} ion. Superpositions between YbeK and the IU-NHs from *C. fasciculata* (PDB code 2MAS), *Leishmania major* (PDB code 1EZR), and YeiK (PDB code 1Q8F) show root mean square distances (rmsd) of 1.09 Å for 285, 1.16 Å for 278, and 1.11 Å for 293 structurally equivalent Cα atoms, respectively. Thus, the structure of YbeK bound to ribose is highly similar to that of all group I NHs determined so far. Instead, the larger structural divergence between group II and group I NHs is confirmed by the comparison with the IAG-NH from *T. vivax* (PDB code 1HOZ) that shows a 1.43 Å rmsd for only 252 structurally equivalent Cα atoms.

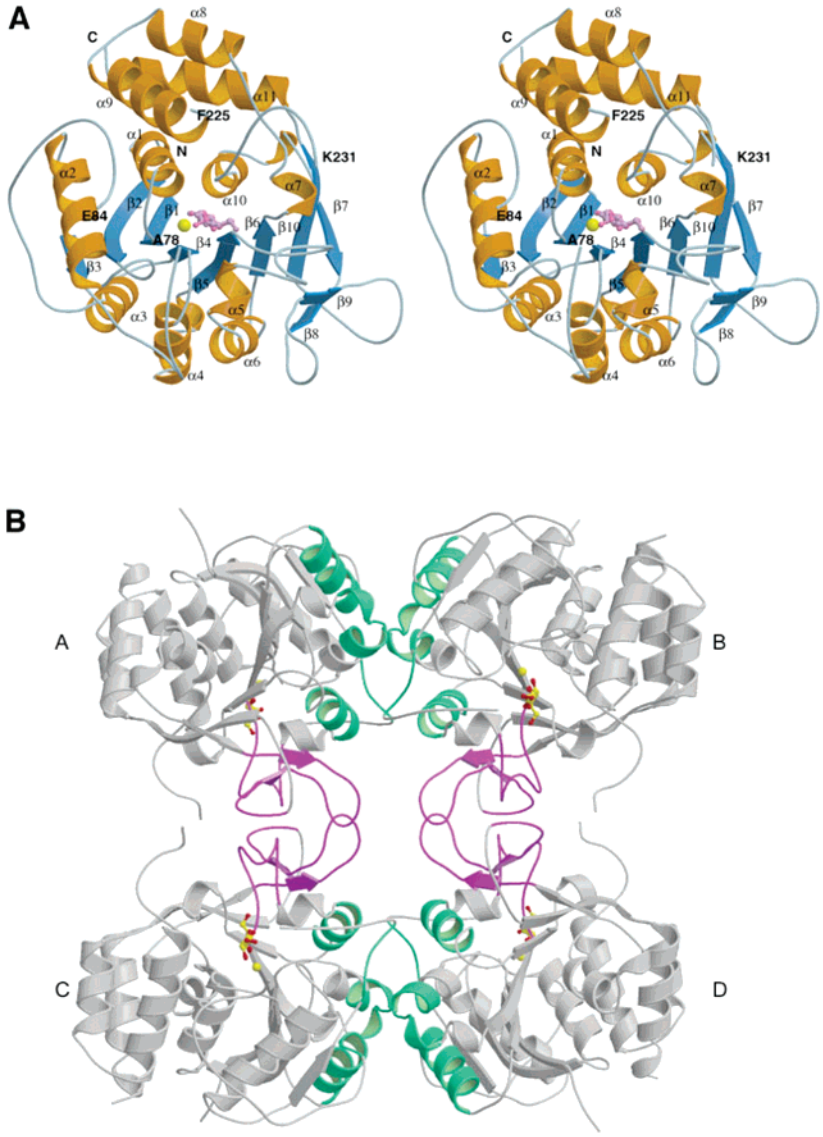

FIGURE 1: Three-dimensional structure of YbeK. (A) Stereoview of the YbeK three-dimensional structure displayed as a ribbon diagram with α-helices colored orange and *β*-strands colored blue. The location of the active site is indicated by the presence of the Ca^{2+} ion depicted as a yellow sphere and of the two anomeric α- and *β*-ribose forms represented as a ball-and-stick model in pink and light pink, respectively. Two amino acid residue stretches, Ala78−Glu84 and Phe225−Lys231, are missing from the model. (B) Tetrameric structure of YbeK. The secondary structure elements involved in the tighter interactions leading to dimers A−C and B−D are colored in violet and include the *β*8−*β*9 region and the loop connecting the C-terminal end of strand *β*5 to the N-terminal end of helix α6. The elements involved in the formation of the second interaction surface (dimers A−B and C−D) are colored in green and include the N-terminal end of the loop connecting strand *β*3 and helix α3, the C-terminal end of helix α4 and the following short loop, and helix α6. The Ca^{2+} ion is depicted as a yellow sphere, and the ligand is represented as a ball-and-stick model. The figures were generated with the programs MOLSCRIPT (*51*) and RASTER3D (*52*).

One YbeK molecule is present in the crystal asymmetric unit, and a tetrameric assembly is generated through the 222 point group symmetry of the orthorhombic space group (Figure 1). The existence of YbeK as a homotetramer in solution is supported by results from gel filtration chromatography and DLS experiments. The intersubunit contacts are mediated by interactions between the same secondary structure elements involved in tetramer formation in IU-NHs and in YeiK (*21*, *22*, *44*). The intersubunit interactions are mainly hydrophobic and complemented with several hydrogen bonds. A total of 1562 $Å^2$ of the accessible surface is buried in each monomer upon formation of the A−C or B−D dimers (Figure 1). This interface includes the *β*8−*β*9 region (residues 261−276) and the loop connecting the C-terminal end of strand *β*5 to the N-terminal of helix α6 (residues 156−161). YbeK allows more extensive interactions between these monomers compared to the corresponding *C. fasciculata* IU-NH (754 $Å^2$) and YeiK (1071 $Å^2$) monomers. The larger buried surface is due to a different orientation of the loop connecting strands *β*8 and *β*9, moving toward the interacting subunit. The second and less prominent subunit interface is established between monomers A−B and C−D, with 848 $Å^2$ of the accessible surface area buried in each monomer upon dimer formation and is comparable with what was observed for the IU-NH from *Crithidia* and the YeiK enzyme (851 and 891 $Å^2$, respectively). Superposition between tetramers of various group I NHs brings forth even larger differences. In fact, when a YbeK tetramer and a YeiK tetramer are superimposed, matching the atoms from a single monomer only, with a rmsd of 1.11 Å for 293 Cα atoms,

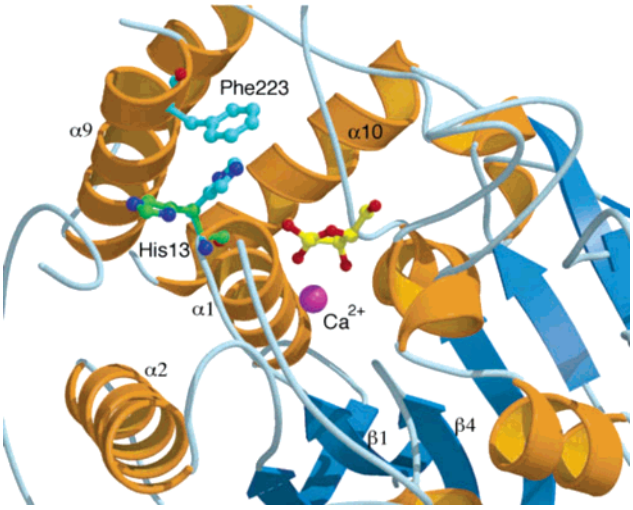

FIGURE 2: A dynamic switch between the open and closed NH structures. Close-up view of the active site of YbeK, with β-strands shown as blue arrows and α-helices as yellow ribbons. Residue His13 can adopt two distinct conformations, and when it assumes the conformation depicted in cyan, it prevents the repositioning of Phe223, part of the highly flexible helix α9, in the active site. Conversely, when His13 is pointing away (depicted in green) from the α9 helix, a small pocket becomes available for Phe223, allowing the bending of the helix toward the substrate. The figure was generated with the programs MOLSCRIPT (*51*) and RASTER3D (*52*).

the same atoms from the corresponding other monomers of each protein show rmsds of 2.00, 3.73, and 5.28 Å. These values reflect a displacement of each monomer with respect to their counterparts. Even larger differences are measured when the IU-NHs from *C. fasciculata* (1.09, 3.16, 4.25, and 7.23 Å for 285 Cα atoms) or *L. major* (1.16, 2.99, 4.43, and 5.32 Å for 278 Cα atoms) are similarly superimposed with the YbeK tetramer. For comparison, rmsd values of 0.8, 1.26, 1.28, and 2.61 Å are calculated for a total of 298 Cα atoms when comparing the two IU-NHs that share a highly similar quaternary structure. Thus, despite the fact that the same tertiary structure elements are responsible for the tetramerization of CU- and IU-NHs, the tetrameric assemblies differ noticeably.

The Active Site of YbeK. The active site of YbeK is located in a cavity at the topological switchpoint of the core β-sheet, lined by residues in strands β1, β2, β4, and β5 and from helices α2 and α9. A Ca^{2+} ion is bound at the bottom of the site, coordinated by the protein through the side chain carboxylates of Asp10, Asp15 (bidentate), and Asp241 and the main chain carbonyl oxygen of Thr124. The 2′- and 3′-hydroxyl groups of the ribose that was cocrystallized with the protein and one ordered water molecule complete the octacoordination sphere of the metal. The portion of the active site of YbeK involved in Ca^{2+} coordination is highly similar to all known NHs, underlining its conserved and crucial role in NH function. The outer half of the cavity is likely responsible for the interactions between the enzyme and the nitrogenous base of the nucleoside substrates. This portion of the active site of YbeK is lined by the hydrophobic side chains of amino acid residues Ala78, Trp159, and Phe165 that could provide binding interactions with the hydrophobic moiety of the bound nucleoside substrate. The hydrophilic side chains of residues Lys231 and His240 extend toward the center of the binding pocket, poised for polar interactions with the hydrophilic substituents in pyrimidine rings.

The outermost portion of the active site of YbeK is not well defined, since no electron density was associated with residues Tyr226, His227, Lys228, Asp229, and Glu230, which are part of the C-terminal portion of helix α9. Moreover, the side chains of residues Phe222, Phe223, Leu224, and Glu225 are more flexible compared to the rest of the protein, as judged by the quality of the electron density and the average temperature factors (45.5 $Å^2$, compared to a 14 $Å^2$ average *B*-factor for protein atoms in the structure). Five residues belonging to the crossover loop connecting the structural elements β3 and α3 (Asp79, Asn80, Val81, His82, Gly83) are also missing in the final model. Structural alignments of YbeK with the protozoan IU-NHs indicate that these amino acids are likely interacting with the nitrogenous base of the substrate. Indeed, the homologous regions of the IU-NH from *C. fasciculata* are also disordered in the ligand-free structure but become ordered upon binding of a transition state-like inhibitor (*23*). The closed conformation of NHs plays a dual role in providing binding interactions with the substrate and shielding the reaction center from the solvent. Thus, the residues omitted in the YbeK model are probably flexible because of their involvement in interactions with the nucleobase that is not present in the YbeK/ribose complex.

Two distinct conformations have been previously observed in NH structures, an open ligand-free form or a closed ligand-bound state (*23*). These structures differ in the conformation of the loop connecting strand β3 to helix α3 and of helix α9 that in the closed form shield the catalytic site from the bulk solvent. The structure of YbeK with bound ribose resembles the features of the open NH conformation, with the β3−α3 loop and C-terminal end of helix α9 flexible, that become ordered only in closed structures where an inhibitor (*23*), a substrate (*45*), or a substrate mimic (*21*) is bound at the active site, reflecting a possible functional role in substrate entry. From the present open structure of YbeK bound to ribose, it thus appears that the interactions with the ribose moiety of the substrate are not sufficient for inducing a complete transition to the closed form of the enzyme and that interactions between the nitrogenous base and the enzyme mediate the stabilization of the closed form. Hence, the "closed" YeiK/glycerol complex that was previously described is therefore probably induced by other factors such as crystal lattice contacts stabilizing this conformation. The transition between the open and closed form in NHs is thus of seminal importance for binding of substrates, for the shielding the reaction center from the free solvent, and also for product release. The mechanistic details of the structural "switch" mediating this transition are yet unknown. A possible mechanism in group I NHs is suggested by the dual conformation of the side chain of His13 observed in YbeK (Figure 2). When His13 is pointing in the active site, its imidazole ring prevents the positioning of Phe223 deep in the binding pocket, in the conformation characteristic of closed NH structures, thus forcing the "open" conformation of helix α9. The second conformation of His13, pointing away from the active site, frees the space for the phenyl ring of Phe223 and allows the relocation of the α9 helix toward the binding site. In the YeiK structure the identical His residue is observed only in the conformation

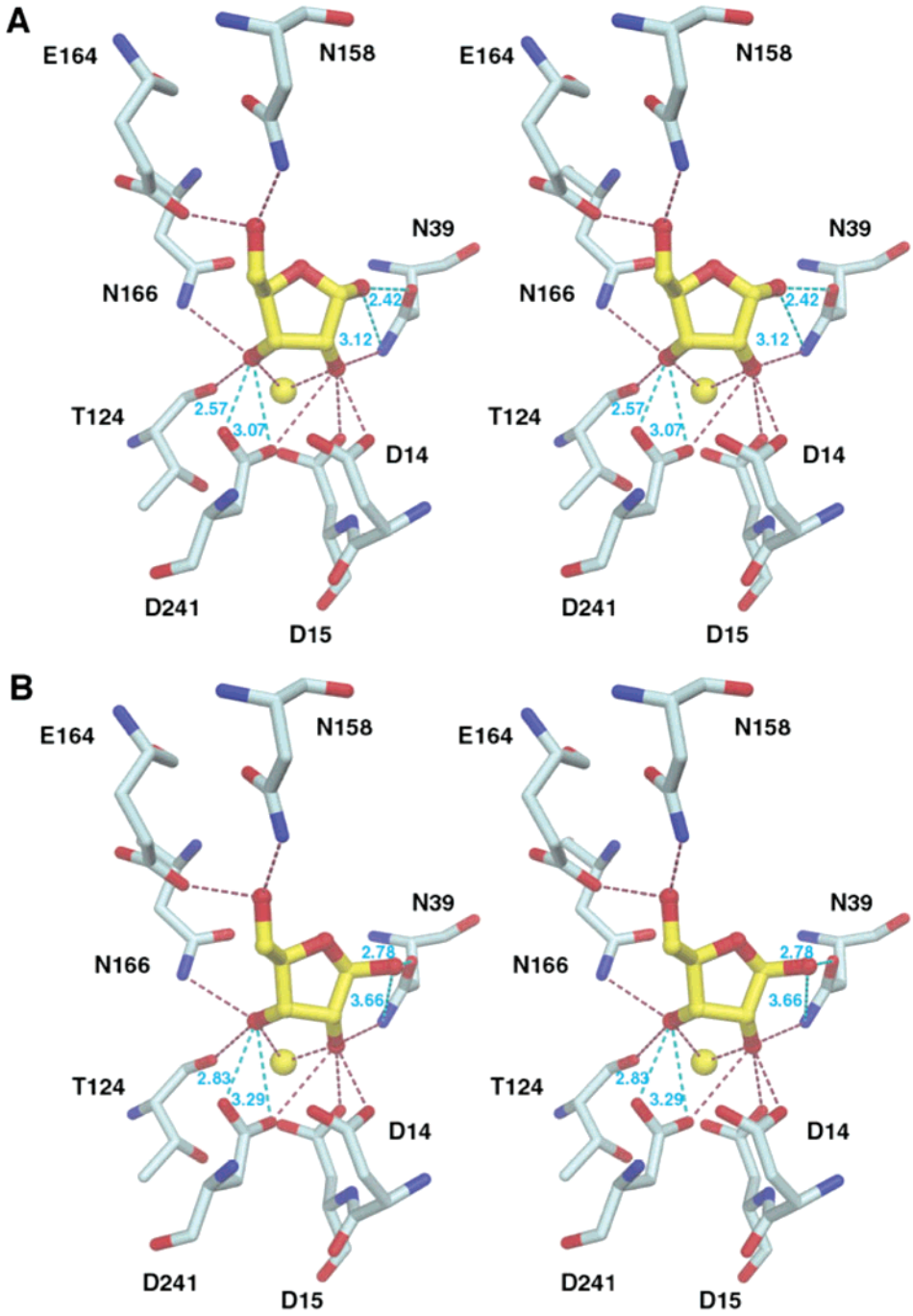

FIGURE 3: Interactions of YbeK with the α and *β* anomers of ribose. (A) Stereoview of the active site interactions between YbeK and *β*-ribose. (B) Same as in (A) for the bound α-ribose molecule. Hydrogen-bonding interactions and calcium coordination are depicted as dashed lines. Protein−ligand distances differing between the two anomers are highlighted (distances expressed in Å), and the corresponding bonds are colored in cyan. Figures generated with DINO (http://www.dino3d.org).

pointing away from the active site, consistent with the closed form adopted by the enzyme (*21*). In the *Crithidia* and *Leishmania* IU-NHs, the His is replaced by a Leu residue that undergoes a similar movement in the transition between the unliganded and ligand-bound structures. In these isozymes, the structural homologue of Phe223 is a Tyr residue that is endowed with highly similar steric and hydrophobic properties. Thus, the high-resolution structure of YbeK provides the first insights in the nature of the structural events that guide the transition from the open to the closed form in group I NHs.

Implications for Product Release in NHs. Single crystals of YbeK were successfully grown in complex with D-ribose, one of the products of the hydrolytic reaction. During the crystallographic refinement it became apparent that both the α and *β* anomeric forms of the pentose were bound to the YbeK molecules in the crystal. Although these two forms are in fast equilibrium in solution, it is clear from the various NH structures that the hydrolytic reaction occurs with inversion of configuration at C1′ and that thus the α-ribose represents the true product of the reaction (*21*, *22*, *24*, *45*). Both anomers are similarly accommodated in the active site of YbeK, with the O5′, O3′, and O2′ hydroxyls establishing several specific hydrogen bonds mediated by conserved residues. In the unliganded NH structures, the hydroxyl groups of ligands are substituted by ordered solvent mol-

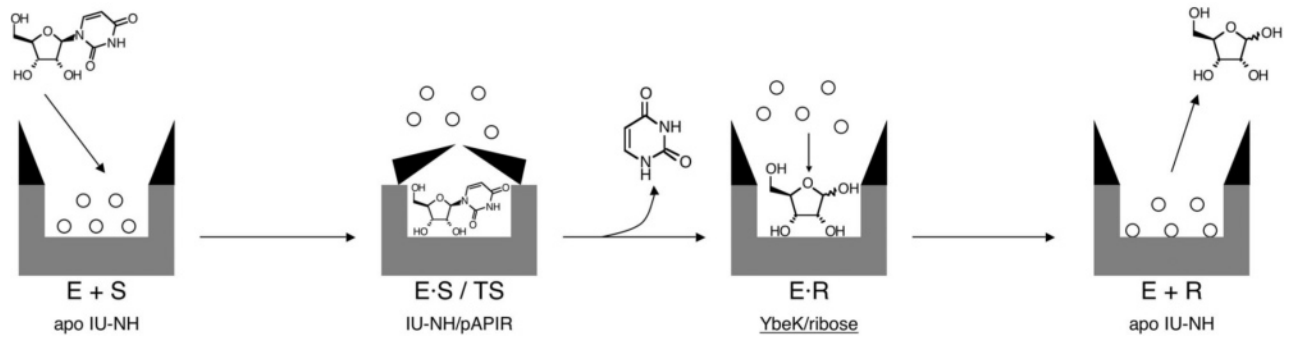

FIGURE 4: The catalytic cycle of group I NHs. Schematic representation of various enzyme states in a catalytic cycle of nucleoside hydrolysis. In the unliganded NH structure (E + S and E + R states, enzyme shown in gray) the active site is occupied by water molecules (depicted as small empty circles), coordinating the Ca^{2+} ion and hydrogen bonded to specific amino acid residues. Binding of the nucleoside substrate (uridine shown here) results in displacement of the ordered solvent and the closure of the β3−α3 loop and of the α9 helix (regions depicted as black triangles) to shield the reaction center from the bulk solvent (E·S/TS). Following release of the nitrogenous base (uracil), the structure transitions to the open form (E·R), allowing access to the active site to the solvent molecules to facilitate product release. NH structures characterized in the individual states are listed.

ecules, hydrogen bonded to the same protein residues. These amino acids include Asp14, Asn39, Thr124, Asn158, Glu164, Asn166, and Asp241 of YbeK and have been proposed to be crucial in ribosyl discrimination and in aiding the geometric distortion to reach the transition state of the hydrolytic reaction. Moreover, the O2′ and O3′ hydroxyl groups complete the coordination sphere of the catalytic Ca^{2+} of YbeK and restrain the conformational freedom of the ligand. The differences in the contacts between YbeK and the α- and β-ribose molecules are limited to the interactions between the Asn39 OD1 and ND2 with the O1′ atom and the Asp241 OD1 and OD2 with the O3′ atom, with the α-ribose molecule involved in shorter hydrogen bonds with the protein (Figure 3). The nucleophilic water molecule in all NH active sites so far characterized is located 3.2−3.3 Å from the C1′ atom, opposite to the scissile N-glycosidic bond. This distance is maintained in YbeK for the β anomer (3.3 Å), whereas for the α form the C1′ atom is further apart from the nucleophile (3.6 Å). In the YbeK crystal structure the catalytic water molecule is fully occupied, thus implying that α-ribose and the nucleophile can simultaneously occupy the active site. Before the present study it was yet unknown whether ribose release from the NH active site was a consequence of less favorable enzyme product interactions or because of competition by the bulk solvent. Overall, the YbeK/product interactions do not differ significantly from the contacts between the sugar and the enzyme in the IU-NH/inhibitor or IAG-NH/substrate complexes. In all of these structures, the ribose hydroxyls are hydrogen bonded at the same spatial position where ordered solvent is present in the unliganded NH structures. The ribosyl moiety of substrate (*45*) or transition state inhibitor (*23*) bound to NHs is distorted toward a C4′-endo conformation that departs significantly from the low-energy C2′- or C3′-endo puckering, a consequence of the enzymatic forces employed for ground-state destabilization. The YbeK-bound ribose also adopts closely related conformations (C4′-endo/O1-exo for the α, C1′-exo/O4′-endo for the β anomer), indicating that the enzyme/ribosyl interaction does not change dramatically during a NH catalytic cycle. These findings imply that the enzyme/base interactions mediate the higher affinity of nucleoside substrates compared to ribose (*46*). Moreover, in the present study we observed the reaction product ribose bound to the open NH structure, a protein conformation that allows access of the catalytic cavity to the bulk solvent. Hence, the competition of water molecules for the subsites occupied by the ribose hydroxyls bound via hydrogen bonds to the enzyme is a likely mechanism for product release in NHs (Figure 4).

Modeling the YbeK/Pyrimidine Base Interactions. The exact mechanisms employed by CU-NHs for implying pyrimidine specificity and leaving group activation are at the present unknown. Protonation of the nucleobase is believed to be a recurring catalytic strategy in NHs to facilitate leaving group departure. For the IU-NH from *C. fasciculata* His241 was proposed as the general acid, protonating the N7 of the hypoxanthine leaving group (*43*). In the purine-specific IAG-NH from *T. vivax* an alternative to general acid catalysis was proposed. Here, the combination of a parallel aromatic stacking interaction with an active site tryptophan and an intramolecular O5′···HC8 hydrogen bond raises the pK_a of the nitrogenous base sufficiently in the active site to allow direct proton transfer from the solvent (*47*, *48*). A very recent kinetic isotope effect study on uridine hydrolysis by the *E. coli* RihC/YaaF protein suggests that the pyrimidine nucleobase could also be activated through enzyme-mediated interactions at the O2 atom (*49*). As an alternative to leaving group protonation, a mechanism could also be envisioned where hydrogen bond donor(s) on the enzyme stabilize the developing negative charge on the nitrogenous base, as is the case in the uracil DNA glycosylases (*50*).

To obtain further information on the residues that could be involved in interactions between the nitrogenous base of nucleosides and YbeK, both for catalysis and specificity, we superimposed its active site with the corresponding active sites of the IU-NH from *C. fasciculata* in complex with the inhibitor pAPIR and of the *E. coli* CU-NH YeiK (Figure 5). The latter structures are representative of the closed conformation. Both hydrophilic and hydrophobic residues line the outer part of the catalytic site, balancing the requirement of stabilizing the aromatic base and discriminating between purine and pyrimidine bases. Amino acids His240 and His82 of YbeK are the only conserved, ionizable active site residues between YbeK and YeiK. In YbeK, His240 could interact through its imidazole moiety with the O2 carbonyl of the pyrimidine ring. This histidine is the structural homologue of His241 of the IU-NH of *C. fasciculata* and of His239 of

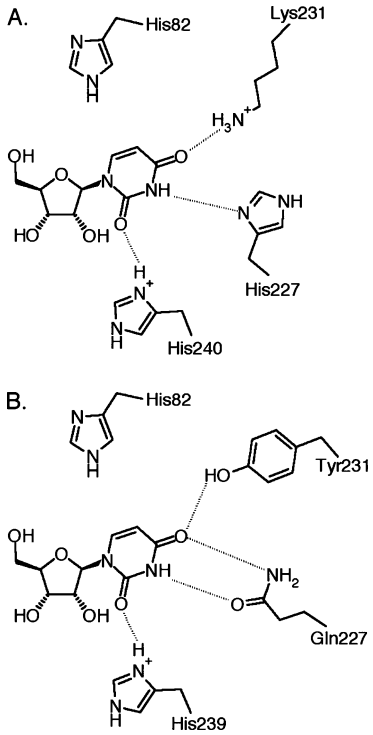

FIGURE 5: Models for CU-NH/nucleoside substrate interactions. (A) Schematic of the active site residues of YbeK and their interactions with the substrate uridine. (B) Schematic of the active site residues of YeiK and their interactions with the substrate uridine. In both panels, dashed lines represent putative hydrogen-bonding and polar interactions that can aid in the discrimination of pyrimidine nucleoside substrates and contribute to leaving group stabilization. A direct interaction between His82 and the N1 atom of uracil could take place after N-glycosidic bond hydrolysis. Both models were obtained through superposition of the YbeK or YeiK structure with the *C. fasciculata* IU-NH complexed with the transition state-like inhibitor pAPIR (*23*). The uridine molecule was modeled as the IU-NH-bound inhibitor.

YeiK. In the IU-NH this residue has been proposed to act as the general acid for the protonation of the purine ring, hence facilitating leaving group departure (*43*). However, in YeiK His239 has been proposed to play a role in the positioning of the nucleic base in a conformation that enhances ground-state destabilization or to allow proton transfer from another general acid (*21*). Residue His82 of YbeK, part of the flexible $\beta3-\alpha3$ loop, could also make a direct interaction with the nucleic base. Remarkably, mutation to alanine or asparagine of both (conserved) histidine residues in YeiK does not result in variations in k_{cat} (*21*). This suggests that the negative charge developing at the pyrimidine base is stabilized by other means and/or by different residues in CU-NHs.

Residue His227 is part of the disordered C-terminal end of helix $\alpha9$ and aligns with Gln227 of YeiK. This residue in YeiK has been proposed to interact with the N3 and O4 atoms of uridine via a bidentate hydrogen bond and to provide a crucial interaction in discriminating between the uridine and cytidine substrates. Since His227 of YbeK cannot be involved in the same type of interaction with the base, it is clear that different mechanisms are employed by CU-NHs to discriminate between substrates. Among the other residues of YbeK that could interact with the pyrimidine base, Lys231 is a candidate to complete the upper part of the active site of YbeK. Lys231 is probably the structural homologue of Tyr231 of YeiK and could interact with the uracil ring of the uridine substrate via a hydrogen bond to the O4 carbonyl oxygen. In the observed open conformation of YbeK, Lys231 is quite distant from the base (~10 Å). However, as established for the protozoan IU-NH, binding of substrate could trigger a complex conformational rearrangement of the YbeK structure. This transition could permit an appropriate hydrogen-bonding geometry that would favor the keto group of uridine over the amino group of cytidine, as inferred from the K_M values. In summary, the active site residues in the $\alpha9$ helix of CU-NHs YbeK and YeiK, supposed to encode the enzymatic substrate specificity via specific enzyme/base interactions, differ considerably in the two enzymes. This finding suggests that qualitatively different interactions are effectively exploited by CU- over IU-NHs to selectively discriminate pyrimidine and purine nucleosides in the catalytic process. A systematic mutagenesis approach will be required in order to define the biochemical basis for the substrate specificity in group I NHs.

ACKNOWLEDGMENT

The authors acknowledge the use of beamline ID14-EH2 at the ESRF (Grenoble, France).

SUPPORTING INFORMATION AVAILABLE

Electron density of the YbeK-bound ribose anomers. This material is available free of charge via the Internet at http://pubs.acs.org.

REFERENCES

1. Nygaard, P. (1983) *Metabolism of Nucleotides, Nucleosides and Nucleobases in Microorganisms*, Academic Press, London.
2. Krenitsky, T. A. (1976) Uridine phosphorylase from *Escherichia coli*. Kinetic properties and mechanism, *Biochim. Biophys. Acta 429*, 352−358.
3. Hammond, D. J., and Gutteridge, W. E. (1984) Purine and pyrimidine metabolism in the trypanosomatidae, *Mol. Biochem. Parasitol. 13*, 243−261.
4. Versées, W., and Steyaert, J. (2003) Catalysis by nucleoside hydrolases, *Curr. Opin. Struct. Biol. 13*, 731−738.
5. Miller, R. L., Sabourin, C. L., Krenitsky, T. A., Berens, R. L., and Marr, J. J. (1984) Nucleoside hydrolases from *Trypanosoma cruzi*, *J. Biol. Chem. 259*, 5073−5077.
6. Dewey, V. C., and Kidder, G. W. (1973) Partial purification and properties of a nucleoside hydrolase from *Crithidia*, *Arch. Biochem. Biophys. 157*, 380−387.
7. Petersen, C., and Møller, L. B. (2001) The RihA, RihB, and RihC ribonucleoside hydrolases of *Escherichia coli*. Substrate specificity, gene expression, and regulation, *J. Biol. Chem. 276*, 884−894.
8. Ogawa, J., Takeda, S., Xie, S. X., Hatanaka, H., Ashikari, T., Amachi, T., and Shimizu, S. (2001) Purification, characterization, and gene cloning of purine nucleosidase from *Ochrobactrum anthropi*, *Appl. Environ. Microbiol. 67*, 1783−1787.
9. Magni, G., Fioretti, E., Ipata, P. L., and Natalini, P. (1975) Baker's yeast uridine nucelosidase. Purification, composition, and physical and enzymatic properties, *J. Biol. Chem. 250*, 9−13.
10. Ribeiro, J. M., and Valenzuela, J. G. (2003) The salivary purine nucleosidase of the mosquito, *Aedes aegypti*, *Insect Biochem. Mol. Biol. 33*, 13−22.
11. Versées, W., Van Holsbeke, E., De Vos, S., Decanniere, K., Zegers, I., and Steyaert, J. (2003) Cloning, preliminary characterization and crystallization of nucleoside hydrolases from *Caenorhabditis elegans* and *Campylobacter jejuni*, *Acta Crystallogr. D59*, 1087−1089.
12. Kim, B. K., Cha, S., and Parks, R. E., Jr (1968) Purine nucleoside phosphorylase from human erythrocytes. II. Kinetic analysis and substrate-binding studies, *J. Biol. Chem. 243*, 1771−1776.

13. Todd, S. J., Moir, A. J., Johnson, M. J., and Moir, A. (2003) Genes of *Bacillus cereus* and *Bacillus anthracis* encoding proteins of the exosporium, *J. Bacteriol. 185*, 3373−3378.
14. Redmond, C., Baillie, L. W., Hibbs, S., Moir, A. J., and Moir, A. (2004) Identification of proteins in the exosporium of *Bacillus anthracis*, *Microbiology 150*, 355−363.
15. Anjum, M. F., Green, J., and Guest, J. R. (2000) YeiL, the third member of the CRP-FNR family in *Escherichia coli*, *Microbiology 146*, 3157−3170.
16. Parkin, D. W., Horenstein, B. A., Abdulah, D. R., Estupiñan, B., and Schramm, V. L. (1991) Nucleoside hydrolase from *Crithidia fasciculata*. Metabolic role, purification, specificity, kinetic mechanism, *J. Biol. Chem. 266*, 20658−20665.
17. Parkin, D. W. (1996) Purine-specific nucleoside *N*-ribohydrolase from *Trypanosoma brucei brucei*. Purification, specificity, and kinetic mechanism, *J. Biol. Chem. 271*, 21713−21719.
18. Pelle, R., Schramm, V. L., and Parkin, D. W. (1998) Molecular cloning and expression of a purine-specific N-ribohydrolase from *Trypanosoma brucei brucei*. Sequence, expression, and molecular analysis, *J. Biol. Chem. 273*, 2118−2126.
19. Estupiñan, B., and Schramm, V. L. (1994) Guanosine-inosine-preferring nucleoside *N*-glycohydrolase from *Crithidia fasciculata*, *J. Biol. Chem. 269*, 23068−23073.
20. Janion, C., and Lovtrup, S. (1963) Pyrimidine nucleoside hydrolase in *Thermobacterium acidophilum*, *Acta Biochim. Pol. 10*, 183−189.
21. Giabbai, B., and Degano, M. (2004) Crystal structure to 1.7 Å of the *Escherichia coli* pyrimidine nucleoside hydrolase YeiK, a novel candidate for cancer gene therapy, *Structure 12*, 739−749.
22. Degano, M., Gopaul, D. N., Scapin, G., Schramm, V. L., and Sacchettini, J. C. (1996) Three-dimensional structure of the inosine-uridine nucleoside N-ribohydrolase from *Crithidia fasciculata*, *Biochemistry 35*, 5971−5981.
23. Degano, M., Almo, S. C., Sacchettini, J. C., and Schramm, V. L. (1998) Trypanosomal nucleoside hydrolase. A novel mechanism from the structure with a transition-state inhibitor, *Biochemistry 37*, 6277−6285.
24. Versées, W., Decanniere, K., Pellé, R., Depoorter, J., Brosens, E., Parkin, D. W., and Steyaert J. (2001) Structure and function of a novel purine specific nucleoside hydrolase from *Trypanosoma vivax*, *J. Mol. Biol. 307*, 1363−1379.
25. Otwinowski, Z., and Minor, W. (1997) *Methods in Enzymology*, Vol. 276, Academic Press, New York.
26. French, S., and Wilson, K. (1978) On the treatment of negative intensity observations, *Acta Crystallogr. A34*, 517−525.
27. Collaborative Computational Project Number 4 (1994) The CCP4 suite: programs for protein crystallography, *Acta Crystallogr. D50*, 760−763.
28. Matthews, B. W. (1968) Solvent content of protein crystals, *J. Mol. Biol. 33*, 491−497.
29. Vagin, A. A., and Teplyakov, A. (1997) Spherically averaged phased translation function and its application to the search for molecules and fragments in electron-density maps, *Acta Crystallogr. D30*, 1022−1025.
30. Perrakis, A., Morris, R., and Lamzin, V. S. (1999) Automated protein model building combined with iterative structure refinement, *Nat. Struct. Biol. 6*, 458−463.
31. Jones, T. A., Zou, J. Y., Cowan, S. W., and Kjeldgaard, M. (1991) Improved methods for building protein models in electron density maps and the location of errors in these models, *Acta Crystallogr. A47*, 110−119.
32. Murshudov, G. N., Vagin, A. A., and Dodson, E. J. (1997) Refinement of macromolecular structures by the maximum-likelihood method, *Acta Crystallogr. D53*, 240−255.
33. McRee, D. (1993) *Practical Protein Crystallography*, Academic Press, San Diego.
34. Winn, M. D., Isupov, M. N., and Murshudov, G. N. (2001) Use of TLS parameters to model anisotropic displacements in macromolecular refinement, *Acta Crystallogr. D57*, 122−133.
35. Laskowski, R. A., MacArthur, M. W., Moss, D. S., and Thornton, J. M. (1993) PROCHECK: a program to check the stereochemical quality of protein structures, *J. Appl. Crystallogr. 26*, 283−291.
36. Hooft, R. W., Vriend, G., Sander, C., and Abola, E. E. (1996) Errors in protein structures, *Nature 381*, 272.
37. Kleywegt, G. J., and Jones, T. A. (1997) *Methods in Enzymology*, Vol. 277, Academic Press, New York.
38. Lawrence, M. C., and Colman, P. M. (1993) Shape complementarity at protein/protein interfaces, *J. Mol. Biol. 234*, 946−950.
39. Mazzella, L. J., Parkin, D. W., Tyler, P. C., Furneaux, R. H., and Schramm, V. L. (1996) Mechanistic diagnoses of N-ribohydrolases and purine nucleoside phosphorylase, *J. Am. Chem. Soc. 118*, 2111−2112.
40. Shapiro, R., and Kang, S. (1969) Uncatalyzed hydrolysis of deoxyuridine, thymidine, and 5-bromodeoxyuridine, *Biochemistry 8*, 1806−1810.
41. Garrett, E. R., and Mehta, P. J. (1972) Solvolysis of adenine nucleosides. I. Effects of sugars and adenine substituents on acid solvolyses, *J. Am. Chem. Soc. 94*, 8532−8541.
42. Horenstein, B. A., Parkin, D. W., Estupiñan B., and Schramm, V. L. (1991) Transition-state analysis of Nucleoside Hydrolase from *Crithidia fasciculata*, *Biochemistry 30*, 10788.
43. Gopaul, D. N., Meyer, S. L., Degano, M., Sacchettini, J. C., and Schramm, V. L. (1996) Inosine-uridine nucleoside hydrolase from *Crithidia fasciculata*. Genetic characterization, crystallization, and identification of histidine 241 as a catalytic site residue, *Biochemistry 35*, 5963−5970.
44. Shi, W., Schramm, V. L., and Almo, S. C. (1999) Nucleoside hydrolase from *Leishmania major*. Cloning, expression, catalytic properties, transition state inhibitors, and the 2.5-Å crystal structure, *J. Biol. Chem. 274*, 21114−21120.
45. Versées, W., Decanniere, K., Van Holsbeke, E., Devroede, N., and Steyaert J. (2002) Enzyme−substrate interactions in the purine-specific nucleoside hydrolase from *Trypanosoma vivax*, *J. Biol. Chem. 277*, 15938−15946.
46. Vandemeulebroucke, A., Versées, W., De Vos, S., Van Holsbeke, E., and Steyaert, J. (2003) Pre-steady-state analysis of the nucleoside hydrolase of *Trypanosoma vivax*. Evidence for half-of-the-sites reactivity and rate-limiting product release, *Biochemistry 42*, 12902−12908.
47. Loverix, S., Geerlings, P. McNaughton, M., Augustyns, K., Vandemeulebroucke A., Steyaert, J., and Versées, W. (2005) Substrate-assisted leaving group activation in enzyme-catalyzed N-glycosidic bond cleavage, *J. Biol. Chem. 280*, 14799−14802.
48. Versées, W., Loverix, S., Vandemeulebrucke, A., Geerlings, P., and Steyaert, J. (2004) Leaving group activation by aromatic stacking: an alternative to general acid catalysis, *J. Mol. Biol. 338*, 1−6.
49. Hunt, C., Gillani, N., Farone, A., Rezaei, M, and Kline, P. C. (2005) Kinetic isotope effects of nucleoside hydrolase from *Escherichia coli*, *Biochim. Biophys. Acta 1751*, 140−149.
50. Drohat, A. C., Jagadeesh, J., Ferguson, E., and Stivers, J. T. (1999) Role of electrophilic and general base catalysis in the mechanism of *Escherichia coli* uracil DNA glycosylase, *Biochemistry 38*, 11866−11875.
51. Kraulis, P. J. (1991) MOLSCRIPT: a program to produce both detailed and schematic plots of protein structures, *J. Appl. Crystallogr. 24*, 946−950.
52. Merritt, E. A., and Murphy, M. E. P. (1994) Raster3D version 2.0: a program for photorealistic molecular graphics, *Acta Crystallogr. D50*, 869−873.

BI0511991